INTERNATIONAL JOURNAL FOR NUMERICAL METHODS IN FLUIDS, VOL. 10, 443–459 (1990)

ON THE REVERSED FLOW AND OSCILLATING WAKE IN AN ASYMMETRICALLY HEATED CHANNEL

T. S. CHANG AND T. F. LIN

Department of Mechanical Engineering, National Chaio Tung University, 1001 Ta Hsueh Road, Hsinchu, Taiwan, R.O.C.

SUMMARY

The detailed processes of flow reversal in a buoyancy-induced flow through a one-side-heated vertical channel of finite height were simulated numerically. It is of interest to note that the wake above the heated plate is oscillatory at high Rayleigh number and there exists a minimum in the transient variation of the average Nusselt number. Additionally, the predicted steady average Nusselt number and induced flow rate are correlated by empirical equations.

KEY WORDS Oscillatory natural convection Vertical channel

INTRODUCTION

Recent interest in buoyancy-induced flow through a heated vertical channel has been mainly activated by its importance in the cooling of microelectronic equipment and the design of plate-type solar collectors. Early studies were concentrated on the symmetrically heated channel of uniform wall temperature or heat flux. Asymmetric heating, however, is often encountered in various applications.

Steady laminar natural convection between two vertical plates maintained at the same uniform temperature was numerically investigated by Bodoia and Osterle.[1] A similar problem with asymmetrically heated walls was considered by Aung *et al.*[2] Later, wall conduction effects were taken into consideration by Burch *et al.*[3] Temporal flow development following a step increase in the wall temperature was examined by Kettleborough[4] and Nakamura *et al.*[5] for symmetric heating. Sparrow and co-workers[6, 7] performed a combined numerical and experimental study on steady laminar natural convection flow in a one-side-heated vertical channel. They observed that adjacent to the upper part of the unheated wall a pocket of recirculating flow was present when Ra/A exceeded a certain value. The reversed flow was conjectured to result from the fluid near the hot wall accelerated by the buoyancy induced by the heated wall, and from the mass conservation requirement that the total mass flow rate at every channel cross-section must be the same. These combined effects dictate that the fluid near the upper part of the cold wall must move downwards. However, the detailed processes on how the reversed flow is formed are not well understood.

The above review clearly indicates that the presence of recirculating flow in an asymmetrically heated channel requires further investigation. The present study aims to unravel the cause of this recirculating flow by conducting a detailed numerical analysis to simulate the transient flow and thermal developments in the channel after a step change in the wall temperature.

The system, as shown schematically in Figure 1, consists of a pair of parallel plates of height L separated by distance $2d$. The gravitational acceleration acts vertically downwards. The dimen-

0271–2091/90/040443–17$08.50

Received 12 December 1988
Revised 13 July 1989

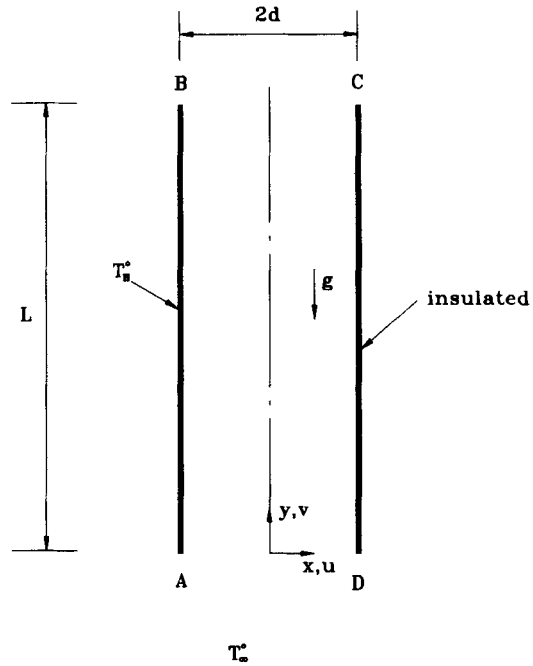

Figure 1. Schematic diagram of the physical system

sions of the plates normal to the x–y plane are very large so that the flow can be treated as two-dimensional. Initially, the quiescent fluid and the channel are at the same uniform temperature T_∞^0. At $t=0$ the temperature at the left plate is suddenly raised to T_H^0 and maintained at this level thereafter, while the right plate is insulated. The fluid adjacent to the left plate is then driven upwards by the buoyancy force resulting from the temperature gradient in the flow, eventually discharging into the ambient at the top of the channel. Meanwhile, ambient fluid is drawn into the lower opening of the channel owing to the pressure defect in the channel. Near the insulated plate the motion of the fluid is primarily influenced by the vigorous flow near the heated wall. To simulate the time evolution of the flow and thermal structure, the full two-dimensional Navier–Stokes equations together with the continuity and energy equations were solved by a numerical scheme derived from the SIMPLER algorithm.[8–10]

MATHEMATICAL FORMULATION

The basic equations describing the transient developments of the momentum and heat transfer in a buoyancy-induced channel flow of a Boussinesq fluid are

$$\frac{\partial}{\partial X}(U) + \frac{\partial}{\partial Y}(V) = 0, \tag{1}$$

$$\frac{\partial}{\partial \tau}(U) + \frac{\partial}{\partial X}(UU) + \frac{\partial}{\partial Y}(UV) = -\frac{\partial P}{\partial X} + \frac{\partial}{\partial X}\left(Pr\frac{\partial U}{\partial X}\right) + \frac{\partial}{\partial Y}\left(Pr\frac{\partial U}{\partial Y}\right), \tag{2}$$

$$\frac{\partial}{\partial \tau}(V) + \frac{\partial}{\partial X}(UV) + \frac{\partial}{\partial Y}(VV) = -\frac{\partial P}{\partial Y} + \frac{\partial}{\partial X}\left(Pr\frac{\partial V}{\partial X}\right) + \frac{\partial}{\partial Y}\left(Pr\frac{\partial V}{\partial Y}\right) + RaPrT, \tag{3}$$

$$\frac{\partial}{\partial \tau}(T) + \frac{\partial}{\partial X}(UT) + \frac{\partial}{\partial Y}(VT) = \frac{\partial}{\partial X}\left(\frac{\partial T}{\partial X}\right) + \frac{\partial}{\partial Y}\left(\frac{\partial T}{\partial Y}\right). \tag{4}$$

In writing the above equations the following non-dimensional variables are introduced:

$$X = \frac{x}{d}, \qquad Y = \frac{y}{d}, \qquad \tau = \frac{t}{d^2/\alpha},$$

$$U = \frac{u}{\alpha/d}, \qquad V = \frac{v}{\alpha/d}, \qquad P = \frac{p - p_\infty}{\rho\alpha^2/d^2},$$

$$T = \frac{T^0 - T^0_\infty}{T^0_H - T^0_\infty}, \quad Pr = \frac{\nu}{\alpha}, \qquad A = \frac{L}{2d}, \tag{5}$$

$$Gr = \frac{g\beta(T^0_H - T^0_\infty)d^3}{\nu^2}, \qquad Ra = GrPr = \frac{g\beta(T^0_H - T^0_\infty)d^3}{\nu\alpha}, \qquad \beta = -\frac{1}{\rho}\frac{\rho - \rho_\infty}{T^0 - T^0_\infty}.$$

For unsteady natural convection in a one-side-heated channel, equations (1)–(4) are subjected to the following initial and boundary conditions:

for $\tau < 0$,

$$T = 0,\ U = V = 0; \tag{6a}$$

for $\tau \geqslant 0$,

$$\text{at } X = -1,\ 0 \leqslant Y \leqslant 2A, \quad T = 1, \quad \text{and} \quad U = V = 0, \tag{6b}$$

$$\text{at } X = +1,\ 0 \leqslant Y \leqslant 2A, \quad \partial T/\partial X = 0 \quad \text{and} \quad U = V = 0, \tag{6c}$$

$$\text{at } X \to \pm\infty, \quad T = 0 \quad \text{and} \quad U = V = 0, \tag{6d}$$

$$\text{at } Y \to \pm\infty, \quad T = 0 \quad \text{and} \quad U = V = 0. \tag{6e}$$

It should be mentioned here that in transient natural convection the heat capacity of the channel walls has significant effects on the flow and thermal characteristics during the transient stage.[11–13] As a preliminary attempt to study the unsteady flow and heat transfer in natural convection in a heated open channel, the channel walls are assumed to be extremely thin so that their heat capacities are relatively small and the thermal boundary conditions on the walls can be represented by equations (6b) and (6c).

Instead of dealing with the infinite computational domain as prescribed above, a finite computational domain is chosen here to reduce the cost of computation. The reduced domain indicated in Figure 2 must be large enough and the boundary conditions at the free boundaries (all the boundaries except CD and JI) should be approximately specified so that the resulting flow and thermal fields are close to those obtained from the infinite domain. The proper size of the extended regions surrounding the inlet and exit ends is determined in the actual numerical computation. The actual boundary conditions employed in the present study are now described in the following.

For the momentum equations:

1. The normal gradients of velocities at all the free surfaces (AB, EF, FG, GH, KL and LA) are zero.
2. The no-slip condition is applied at the solid (CD and JI) and artificial surfaces (BC, JK, HI and DE). (The 'artificial surfaces' denotes the surfaces which do not physically exist, but for the convenience of computation we suppose they do exist.)

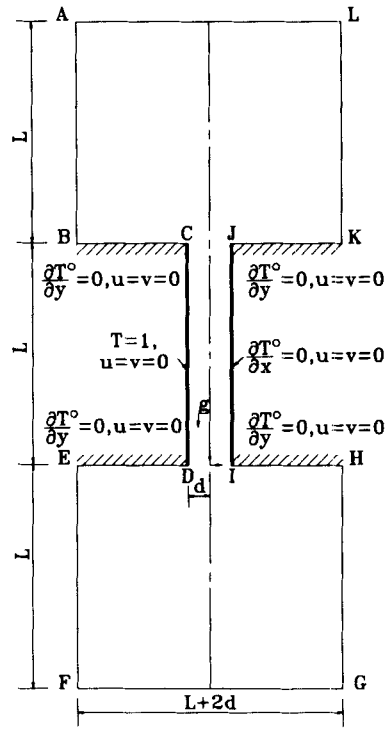

Figure 2. Computational domain and boundary conditions

For the energy equation:

1. The left wall stays at a constant and uniform temperature T_H^0 and the right wall is insulated.
2. At the free surfaces, if the fluid flows out of the computational domain the local temperature gradients in the normal direction are zero; if the flow enters the domain the local temperature is equal to the ambient temperature.
3. At the artificial surfaces the gradients are zero.

The characteristics of heat transfer are expressed by the local and average Nusselt numbers defined as

$$Nu_Y = h_y(2d)/k, \tag{7}$$

$$\overline{Nu} = h_m(2d)/k, \tag{8}$$

where the convective heat transfer coefficients h_y and h_m are defined as

$$h_y = \frac{-k(\partial T^0/\partial x)_{wall}}{T_H^0 - T_\infty^0}, \tag{9}$$

$$h_m = \frac{1}{L}\int_0^L h_y \, dy. \tag{10}$$

In terms of the non-dimensional variables, the local and average Nusselt numbers can be written as

$$Nu_Y = -2(\partial T/\partial X)_{wall}, \tag{11}$$

$$\overline{Nu} = -\frac{1}{A}\int_0^{2A} (\partial T/\partial X)_{\text{wall}}\, \mathrm{d}Y. \tag{12}$$

The characteristics of the flow field are expressed by the inlet Reynolds number, indicating whether the flow is laminar or turbulent. It is defined as

$$Re = \frac{\rho v_{\text{m}}(4d)}{\mu} = \frac{4V_{\text{m}}}{Pr}, \tag{13}$$

where v_{m} is the dimensional average inlet velocity. The hydraulic diameter, which is twice the channel spacing, is used as the characteristic length.

NUMERICAL SCHEME

Because of the elliptic nature of the flow, equations (1)–(4) were solved by a numerical scheme derived from the SIMPLER (semi-implicit method for pressure-linked revised) algorithm developed by Spalding and Patankar.[8–10] The finite difference equations were obtained by integrating the momentum and energy equations over the control volumes defined on a staggered grid system. For instance, the finite difference equation derived from integrating equation (2) for a typical control volume has the form

$$\frac{U_{i,j}^{n+1} - U_{i,j}^{n}}{\Delta\tau}\Delta X_i \Delta Y_j + J_{\text{e}}^{n+1} - J_{\text{w}}^{n+1} + J_{\text{n}}^{n+1} - J_{\text{s}}^{n+1} = (P_{\text{w}}^{n+1} - P_{\text{e}}^{n+1})\Delta Y_j. \tag{14}$$

Here all the momentum fluxes across the control surfaces (the Js) are evaluated approximately by the power-law scheme.[8,9] Also notable in equation (14) is the use of backward difference to approximate the unsteady term and hence the scheme is fully implicit in time. Similar expressions can be obtained for equations (3) and (4). The finite difference equation for the pressure was derived by integrating the continuity equation over its control volume; the velocities in this expression were replaced by equation (14) for U and a similar equation for V.

To obtain enhanced accuracy, non-uniform grids were placed in the computational domain. The grid density is highest in the regions near the channel walls and near the inlet ($y=0$) and exit ($y=L$) of the channel. A total of 60×90 grid lines were used to cover the whole computational domain, among which 16×36 lines were placed inside the channel ($0 \leqslant y \leqslant L$). To be more specific, inside the channel ΔX is varied from 0·0833 to 0·176 and ΔY from 0·144 to 0·48; while in the extended regions surrounding the top and bottom ends ΔX ranges from 0·0833 to 0·378 and ΔY from 0·144 to 0·48. A line-by-line method[14] with iteration was employed to solve the systems of algebraic equations obtained from discretizing the momentum and energy equations and the pressure equation. To account for the drastic variations of the flow and thermal fields during the initial transient, non-uniform time steps are used. In the beginning $\Delta\tau_1$ is set to be in the range from 10^{-3} to 10^{-4} depending on the Rayleigh number. It is gradually increased to about $5\Delta\tau_1$ as the steady state approaches.

The sequence of operations can be briefly stated as follows.

1. Use the known velocity and temperature at time step n as initial guesses for the solutions at time step $n+1$.
2. Solve the pressure equation.
3. Solve the finite difference equations for U and V.
4. Solve the finite difference equation for T.
5. Treat the obtained U, V and T as new guesses and repeat procedures (2–5) until the mass

imbalance compared with the induced flow rate at that step for each control volume is below 10^{-3}; that is, until

$$\frac{|(U_{i+1,j}^{k+1} - U_{i,j}^{k+1})\Delta Y_j - (V_{i,j+1}^{k+1} - V_{i,j}^{k+1})\Delta X_i|}{|U_{i,j}^{k+1}\Delta Y_j| + |V_{i,j}^{k+1}\Delta X_i|} < 10^{-3} \tag{15}$$

for every control volume. In addition, the relative differences in U, V and T at each node between two consecutive iterations are required to be below 10^{-3}; that is,

$$\frac{\max|\phi_{i,j}^{k+1} - \phi_{i,j}^{k}|}{\max|\phi_{i,j}^{k+1}|} < 10^{-3} \tag{16}$$

where ϕ stands for U, V or T.

6. Repeat procedures 1–5 from the onset of the transient to the final steady state.

It should be pointed out that since converged solutions are obtained at each time step, the pressure correction equation normally employed by the SIMPLER algorithm was not used and velocity correction was not required.

The proposed numerical algorithm was validated in two ways. First, the numbers of grid lines in both the X- and Y-direction were doubled. The differences in U, V and T at all grid points obtained from the 60×90 and 120×180 grid systems were less than 2%. Therefore the 60×90 grid was used in the computation of the various cases to be presented. In addition, several different sizes of the extended domains surrounding the inlet and exit ends were tested. The computed results indicate that the regions attached to the ends should each have dimension $(L+2d) \times L$ when $Ra = 10^6$ and $A = 10$ for air. In all the subsequent computations the extended regions of size $(L+2d) \times L$ are considered to be sufficient to simulate the infinite domain. Secondly, the fluid flow and heat transfer phenomena immediately after the wall temperature is raised are governed by one-dimensional heat conduction. The predicted velocity and temperature profiles at early transient for $Ra = 10^6$, $A = 5$ and $Pr = 0{\cdot}7$ are compared with the one-dimensional transient solution of Schetz and Eichhorn[15] for unsteady natural convection on a single vertical plate.[16] Our predictions are in good agreement with the 1D solution. To further validate our numerical scheme, the steady temperature distributions at several Y-locations for $Ra = 10^6$ and $A = 5$ are contrasted with the similarity solution of Ostrach[17] for a natural convection boundary layer over an infinite vertical plate. Good agreement is again noted. Through these program tests the proposed numerical scheme is considered to be appropriate for the problem under investigation.

DISCUSSION OF RESULTS

As indicated by the problem formulation, flow and heat transfer in an asymmetrically heated vertical channel are governed by three non-dimensional groups: the Prandtl number, Rayleigh number and aspect ratio of the channel. Results were obtained for air ($Pr = 0{\cdot}7$) with Ra varying from 10^3 to 10^6 and A from 5 to 10. Particular attention is paid to examining temporal developments of the flow and thermal structures to illustrate the formation of the recirculating flow. In addition, the transient variations of the local and average heat transfer coefficients and the amount of air drawn into the channel through the action of the buoyancy force are also examined.

Evolution of flow and thermal structures

Figures 3(a)–3(d) present the unsteady velocity and temperature fields through isocontour plots for $Ra = 10^3$ and $A = 5$ from the initiation of the transient to the final steady state. The results in

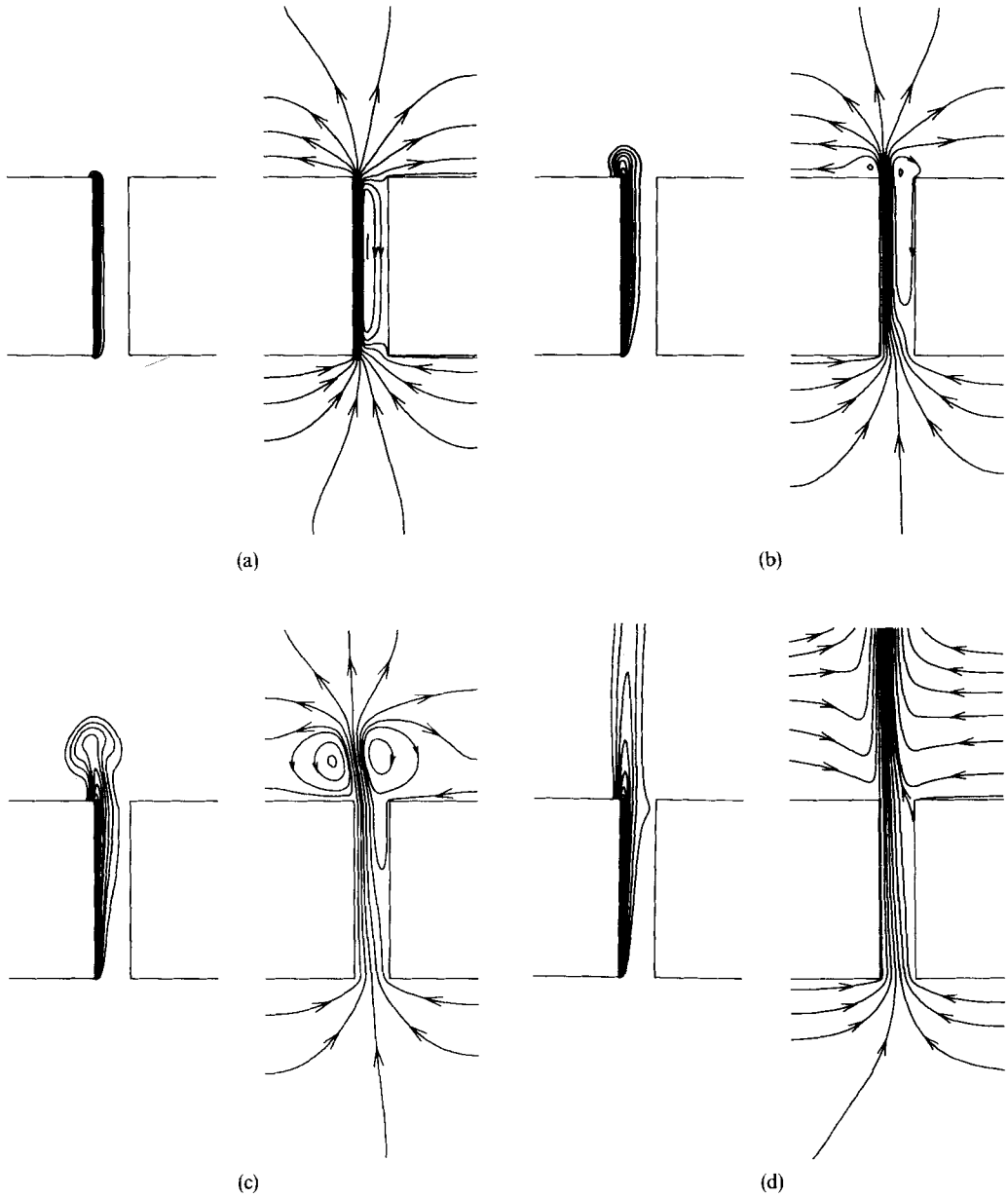

Figure 3. Evolution of the isotherms and streamlines toward the steady state for $Pr=0{\cdot}7$, $A=5$ and $Ra=10^3$: (a) $\tau=0{\cdot}061$, (b) 0·205, (c) 0·361, (d) 2·664

Figure 3(a) clearly indicate that as the left plate is suddenly heated, the fluid in a thin layer adjacent to the plate is driven up by the buoyancy force and expands at the top into the ambient. Accompanying the buoyancy-induced flow motion is the pressure defect in the channel, which in turn draws ambient air into the channel from all directions at the bottom. At the outer edge of the thin layer the fluid does not possess enough momentum to expand into the ambient. Instead, it makes a turn at the top and thus a weakly circulating cell is formed.

The thermal buoyancy layer on the hot plate gradually becomes thicker. The loop-like isotherms at the exit end are the consequence of the outward flow expansion there. The fluid adjacent to the heated plate gradually speeds up owing to the continuing action of the buoyancy force, resulting in significant viscous shearing force which then drags the weakly recirculating cell upwards (Figure 3(b)). The portion of the cell outside the channel slowly grows in size. A new cell is formed just outside the top to the left of the heated plate, again clearly resulting from the

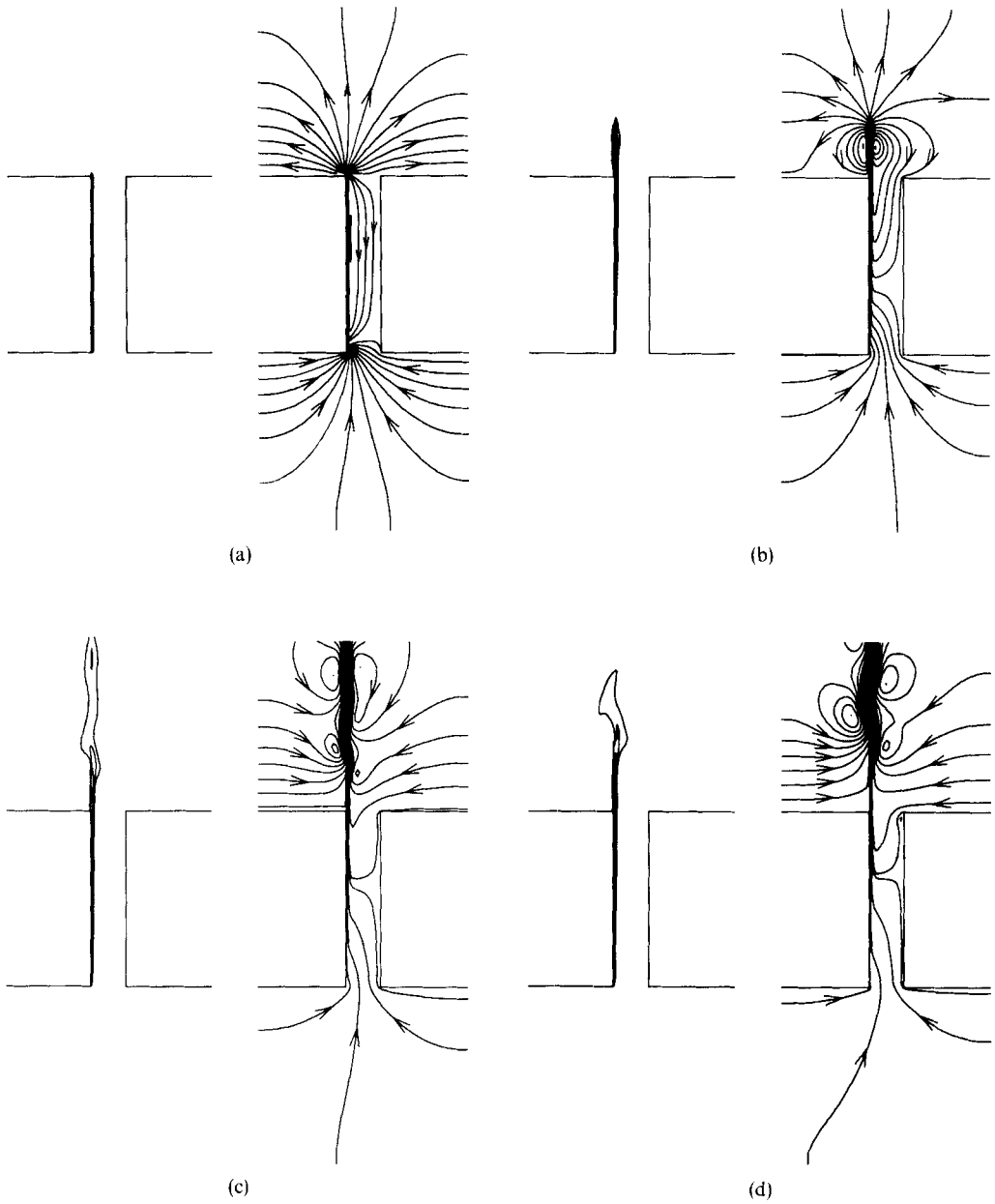

Figure 4. (a–d)

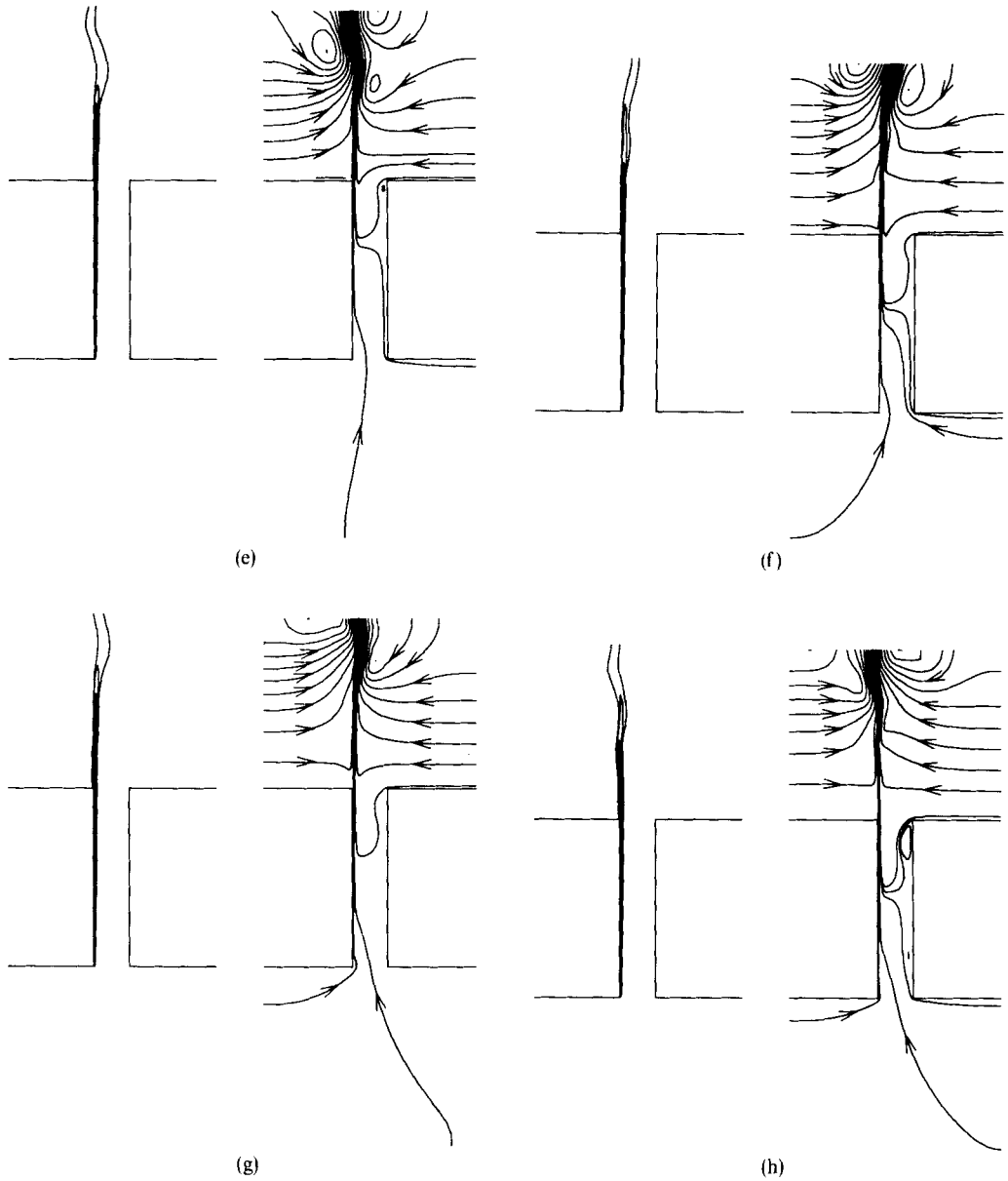

Figure 4. Temporal development of the isotherms and streamlines toward the steady state for $Pr = 0{\cdot}7$, $A = 5$ and $Ra = 10^6$: (a) $\tau = 0{\cdot}0022$, (b) 0·0082, (c) 0·0162, (d) 0·0222, (e) 0·0282, (f) 0·0382, (g) 0·0592, (h) 0·0794

outward flow expansion (Figure 3(b)). This newly formed cell also gradually increases in size (Figure 3(c)).

It is interesting to observe that the cell originally inside the channel is not completely dragged out of the channel (Figures 3(a)–3(c)). Even after reaching the steady state (Figure 3(d)), air surrounding the top opening can be drawn into the channel and moves downwards along the upper part of the insulated plate before turning upwards and moving out of the channel. This downward flow reversal in the upper region near the unheated plate is in congruence with the

experimental observation of Sparrow *et al.*[7] The flow reversal apparently results from the streamlines tilting to the left plate owing to the one-side heating. The complex flow pattern near the exit results in the unusual isotherms in this region (Figures 3(c) and 3(d)).

Heat transfer from the heated plate to the flow at the early transients ($\tau \leqslant 0{\cdot}097$) is mainly due to conduction because the flow in the channel still moves slowly. Later, convection effects set in and a convection-type thermal boundary layer is formed. The flow and heat transfer reach an unvarying state for $\tau \geqslant 2{\cdot}664$.

To investigate the influence of the Rayleigh number change on the time development of the flow and thermal fields, Figures 4(a)–4(h) show the isotherms and streamlines at a number of time steps from the very early transient to the final asymptotic state for $Ra = 10^6$. Comparing Figures 4(a)–4(h) with Figures 3(a)–3(d) indicates that the temporal evolution of the flow and thermal fields at $Ra = 10^3$ and $Ra = 10^6$ is basically similar. Careful scrutiny of the results presented in these figures, however, discloses that several important differences in the evolution of the velocity and temperature fields do exist when Ra is raised from 10^3 to 10^6. First, the velocity and temperature boundary layers at all the transient stages induced by the buoyancy force are much thinner for the case with $Ra = 10^6$. Obviously, the weakly recirculating cell at the early transient (Figures 4(a)) is correspondingly larger and the flow reversal now occurs in a larger region for $\tau \geqslant 0{\cdot}0082$. Secondly, the larger buoyancy force associated with $Ra = 10^6$ draws a larger amount of air into the channel through the bottom and the streamlines in the entry region are greatly distorted. Furthermore, for $Ra = 10^6$ all the recirculating cells develop much sooner. Multiple cells appear in the wake region above the heated plate (Figure 4(c)). Finally, it is important to point out that at $Ra = 10^6$ the wake becomes oscillatory when $\tau \geqslant 0{\cdot}0282$. This can be seen from the isotherms and streamlines given in Figures 4(e)–4(h). The oscillation period is about $\tau_p = 0{\cdot}01$–$0{\cdot}02$. This oscillation in wake, however, does not have significant effects on the heat transfer from the heated plate to the flow in the channel.

To illustrate quantitatively the effects of the Rayleigh number on the transient fluid flow and heat transfer characteristics in the system, in Figures 5–8 we present the velocity and temperature

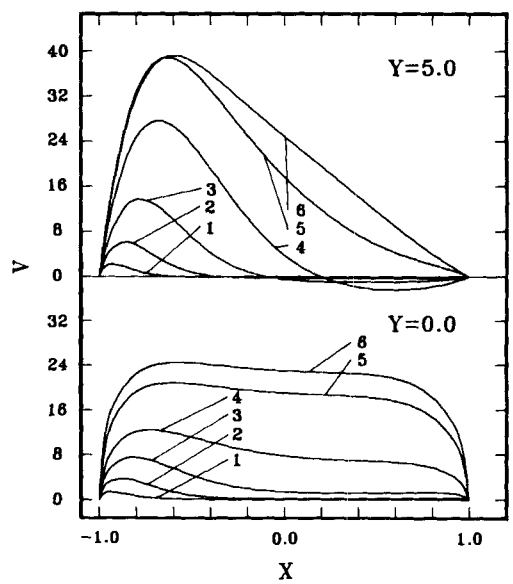

Figure 5. Unsteady development of velocity profiles at the bottom and mid-height for $Pr = 0{\cdot}7$, $A = 5$ and $Ra = 10^3$: (1) $\tau = 0{\cdot}013$, (2) 0·037, (3) 0·085, (4) 0·181, (5) 0·373, (6) 2·664

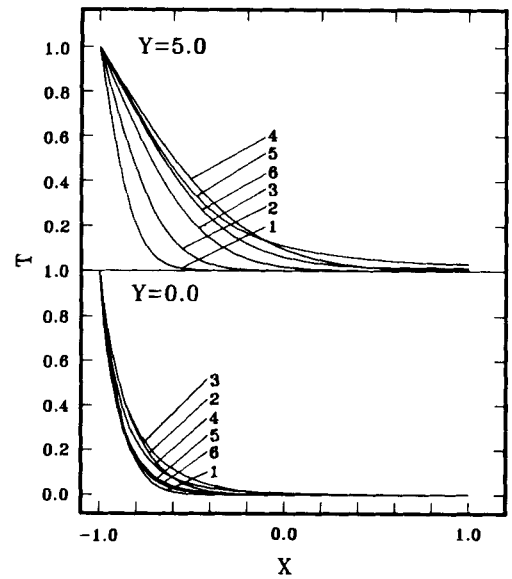

Figure 6. Unsteady development of temperature profiles at the bottom and mid-height for $Pr=0{\cdot}7$, $A=5$ and $Ra=10^3$: (1) $\tau=0{\cdot}013$, (2) 0·037, (3) 0·085, (4) 0·181, (5) 0·373, (6) 2·664

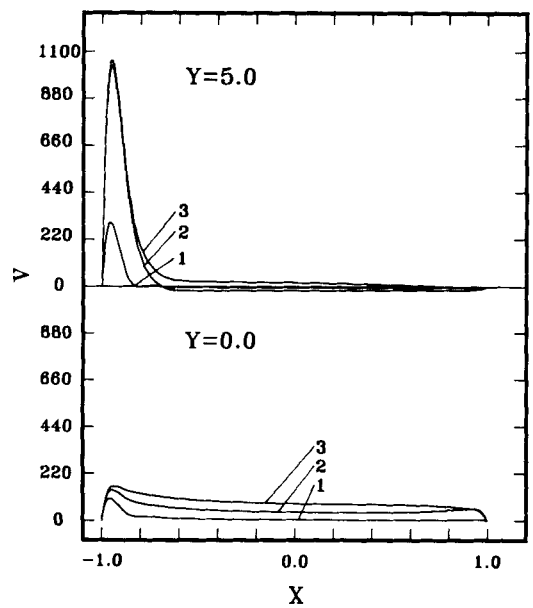

Figure 7. Unsteady development of velocity profiles at the bottom and mid-height for $Pr=0{\cdot}7$, $A=5$ and $Ra=10^6$: (1) $\tau=0{\cdot}0022$, (2) 0·062, (3) 0·0794

profiles at the bottom ($Y=0$) and mid-height ($Y=5$) at selective time steps for $Ra=10^3$ and $Ra=10^6$. The existence of a weakly recirculating cell in the channel adjacent to the unheated plate at the early transient is clearly seen in Figures 5 and 7. The inlet velocity profiles ($Y=0$) at steady state are neither uniform nor parabolic, nor would they be expected to be; in fact, the profiles exhibit maxima near the left wall and the non-uniformity in the velocity profiles becomes more

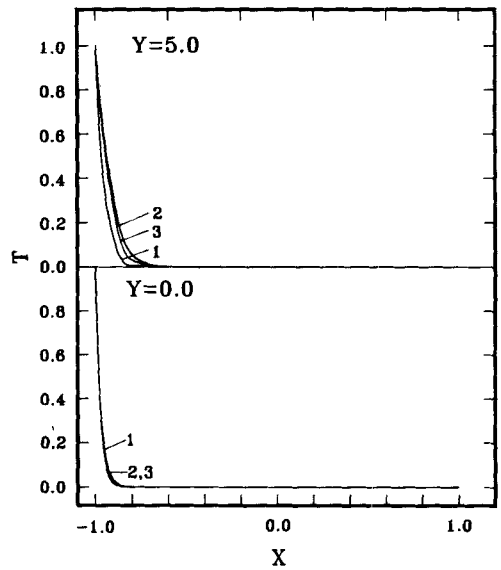

Figure 8. Unsteady development of temperature profiles at the bottom and mid-height for $Pr = 0{\cdot}7$, $A = 5$ and $Ra = 10^6$: (1) $\tau = 0{\cdot}0022$, (2) 0·062, (3) 0·0794

pronounced for a higher Ra (Figure 7). The temporary overshoot of the temperature profiles is noted in Figures 6 and 8 and the transient thermal boundary layers along the heated plate are much thinner for the system with $Ra = 10^6$. Comparing Figure 5 with Figure 7 indicates clearly that at $Ra = 10^6$ the fluid in the channel is driven to a much higher velocity.

Since at $Ra = 10^6$ the velocity and temperature wakes above the heated plate are oscillatory at larger τ, it is conjectured that the velocity and temperature fields inside the channel are also oscillatory at this high Rayleigh number. To clear up this point, the variations of velocity and temperature with time at a number of locations inside the hydrodynamic and thermal boundary layers were examined for $Ra = 10^6$. The results indicate that there are overshoots in both velocity and temperature at all locations considered, but no flow and thermal oscillations were noted.

Nusselt numbers and induced flow rates

The distributions of local Nusselt number along the channel are shown in Figures 9 and 10 for various times and for $Ra = 10^3$ and 10^6 respectively. For a given τ, Nu_Y falls significantly with Y in the region near the bottom, exhibiting the importance of the convection effects. As time elapses, this region gradually extends upwards. The convection effects are more pronounced for $Ra = 10^6$. Beyond this region conduction is dominant and Nu_Y stays constant at a given τ. A rise in Nu_Y near the top ($Y = 2A$) is due to the exit effect from the finite channel. At a given Y-location Nu_Y decreases drastically with time when τ is small. Later, the decrease in Nu_Y with time becomes more and more gradual and finally reaches a steady state value. Higher Nu_Y results for $Ra = 10^6$. The temporal variations of the average Nusselt number from the heated plate to the flow in the channel, shown in Figures 11 and 12 for various Rayleigh numbers, indicate that for a given Ra the Nusselt number quickly decreases with τ at the early stage of the transient, reaches a minimum and then gradually increases toward steady values. The dip in the $\overline{Nu}$–τ curve becomes more pronounced for a higher Ra. The appearance of these dips is evidently due to the overshoot of temperature profiles during the transient stage. When $\tau \to 0$ all $\overline{Nu}$ curves coincide, indicating

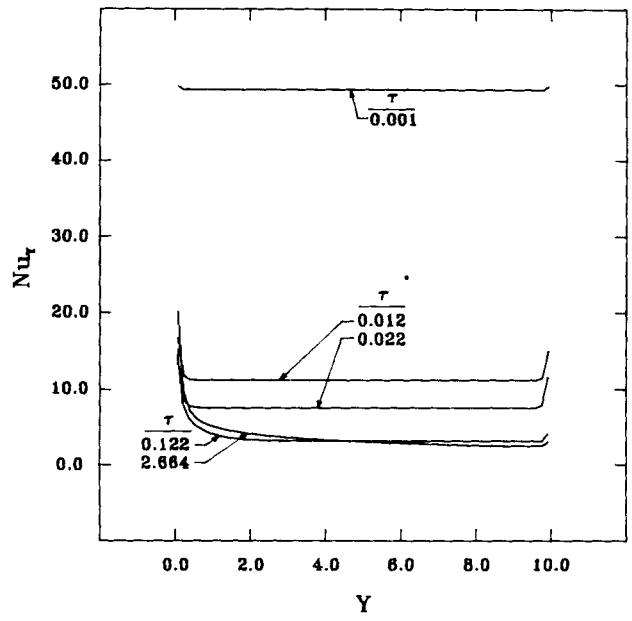

Figure 9. Variation of the local Nusselt number distribution with time for $Pr = 0{\cdot}7$, $A = 5$ and $Ra = 10^3$

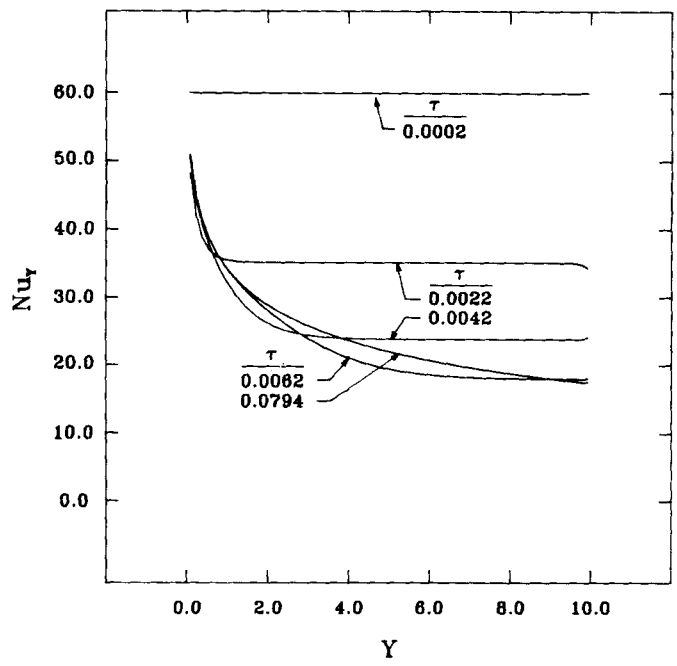

Figure 10. Variation of the local Nusselt number distribution with time for $Pr = 0{\cdot}7$, $A = 5$ and $Ra = 10^6$

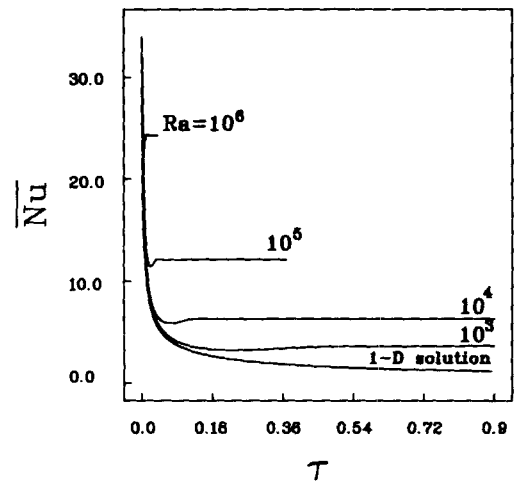

Figure 11. Transient variation of the average Nusselt number at various Rayleigh numbers for $A = 5$

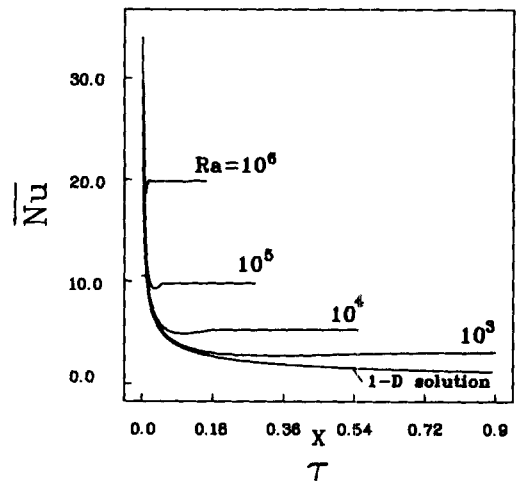

Figure 12. Transient variation of the average Nusselt number at various Rayleigh numbers for $A = 10$

that heat transfer in the flow is conduction-dominant. It is of interest to note that for a fixed Ra the increase A from 5 to 10, by comparing Figure 11 with Figure 12, results in a decrease in $\overline{Nu}$.

The predicted average Nusselt number at steady state is plotted in Figure 13 against a modified Rayleigh number Ra^* defined as Ra/A. The adoption of Ra^* here is simply because the results for steady $\overline{Nu}$ for channels with different aspect ratio can be easily correlated by a single equation. All the predicted data are well correlated by the equation

$$\overline{Nu} = 0{\cdot}86(Ra^*)^{1/4} \quad \text{for } 10^2 \leqslant Ra^* \leqslant 2 \times 10^5. \tag{17}$$

The induced flow rate in the channel by the buoyancy force is valuable in the thermal design of various systems. Figure 14 gives the induced Reynolds number at the inlet at steady state for various Ra. For $A = 10$ the air flow rate increases almost linearly with Ra on a log–log plot, while for $A = 5$ Re only increases slightly when Ra is raised from 10^3 to 10^4. Larger increases in Re result

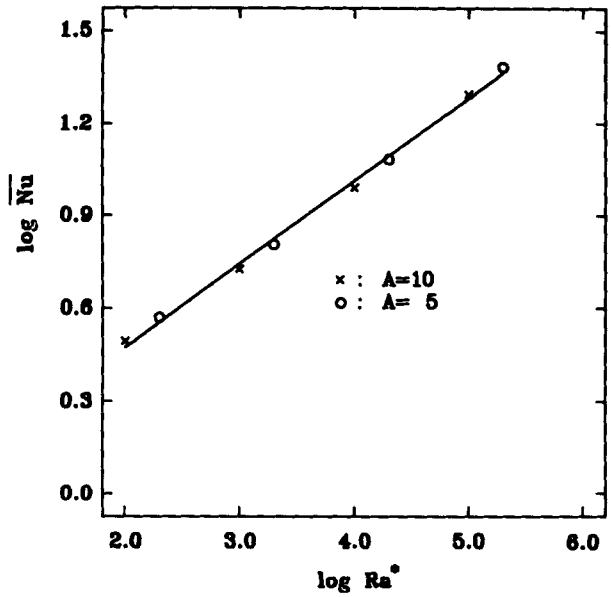

Figure 13. Steady Nusselt number variation with the modified Rayleigh number for $A=10$ (×) and $A=5$ (○)

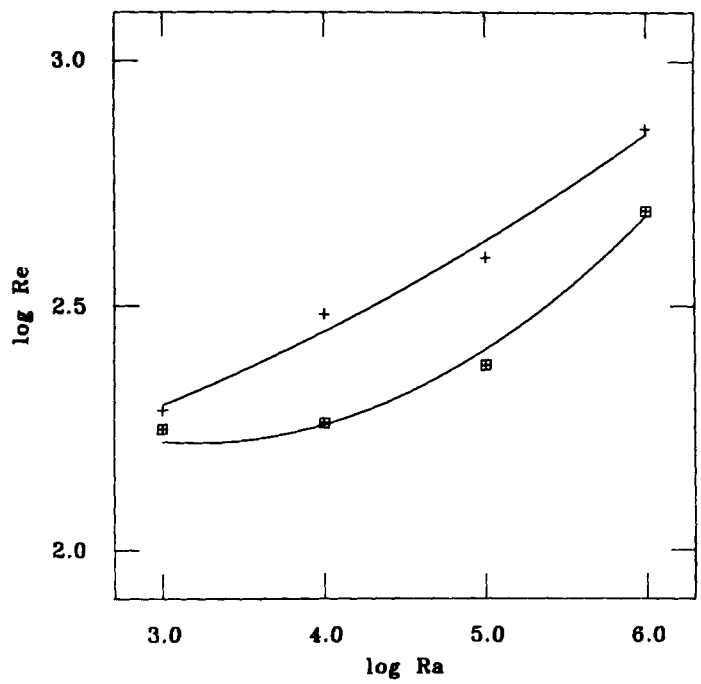

Figure 14. Effect of the Rayleigh number on the inlet Reynolds number at steady state for $A=10$ (+) and $A=5$ (⊞)

for a higher Ra. The predicted air flow rate can be correlated by the following equations:

$$\log Re = 2{\cdot}82 - 0{\cdot}375 \log Ra + 0{\cdot}0587 (\log Ra)^2 \quad \text{for } A = 5, \tag{18}$$

$$\log Re = 2{\cdot}05 + 0{\cdot}0331 \log Ra + 0{\cdot}0168 (\log Ra)^2 \quad \text{for } A = 10. \tag{19}$$

CONCLUDING REMARKS

The detailed processes of the formation of the recirculation flow in buoyancy-induced flow through a one-side-heated vertical channel of finite height were described. At $Ra = 10^6$ the velocity and temperature wakes above the heated plate are oscillatory after a certain τ. Additionally, we noted that temperature overshoot in the thermal boundary layer results in a dip in the transient variation of $\overline{Nu}$.

As already mentioned, the heat capacities of the plate, although ignored in the present study, are expected to have a profound influence on the transient natural convection. This heat capacity effect needs to be examined. Results for various fluids and inclined channels will also be important in many applications.

ACKNOWLEDGEMENTS

The financial support of this research by the Engineering Division, National Research Council of Taiwan, R.O.C. (NSC76-0401-E009-06) is greatly appreciated.

APPENDIX: NOMENCLATURE

A	aspect ratio of the channel, $L/2d$
d	half-interspace of the channel
g	gravitational acceleration
Gr	Grashof number, $g\beta(T_H^0 - T_\infty^0)d^3/\nu^2$
h_y	local heat transfer coefficient, $-k(\partial T^0/\partial x)_{x=-d}/(T_H^0 - T_\infty^0)$
h_m	average heat transfer coefficient, $(1/L)\int_0^L h_y \mathrm{d}y$
J	momentum flux across a control surface
k	thermal conductivity of fluid
L	height of the channel
Nu_y	local Nusselt number, $h_y(2d)/k$
$\overline{Nu}$	average Nusselt number, $h_m(2d)/k$
p	dimensional pressure
P	dimensionless pressure, $(p - p_0)/(\rho\alpha^2/d^2)$
Pr	Prandtl number, ν/α
Ra	Rayleigh number, $Gr\,Pr$
Re	Reynolds number, $\rho v_m(4d)/\mu$
t	time
T	dimensionless temperature, $(T^0 - T_\infty^0)/(T_H^0 - T_\infty^0)$
T^0	temperature
u	velocity in x-direction
U	dimensionless velocity in x-direction, $u/(\alpha/d)$
v	velocity in y-direction
V	dimensionless velocity in y-direction, $v/(\alpha/d)$
x, y	Cartesian co-ordinates

X, Y	dimensionless Cartesian co-ordinates, x/d and y/d
α	thermal diffusivity
β	coefficient of volumetric thermal expansion
μ	dynamic viscosity
ν	kinematic viscosity
ρ	density
τ	dimensionless time
$\Delta\tau$	increase in τ

Subscripts

e, w, n, s	quantities from east, west, north and south surfaces
H	highest value
i, j	indexes for X- and Y-direction
m	mean value
y	local value at location y
∞	ambient value

Superscripts

n	value for the nth time step
k	kth iteration

REFERENCES

1. J. R. Bodoia and J. F. Osterle, 'The development of free convection between heated vertical plates', *J. Heat Transfer*, **84,** 40–44 (1962).
2. W. Aung, L. S. Fletcher and V. Sernas, 'Developing laminar free convection between vertical flat plates with asymmetric heating', *Int. J. Heat Mass Transfer*, **15,** 2293–2308 (1972).
3. T. Burch, T. Rhodes and S. Acharya, 'Laminar natural convection between finitely conducting vertical plates', *Int. J. Heat Mass Transfer*, **28,** 1173–1186 (1985).
4. C. F. Kettleborough, 'Transient laminar free convection between heated vertical plates including entrance effects', *Int. J. Heat Mass Transfer*, **15,** 883–896 (1972).
5. H. Nakamura, Y. Asako and T. Naitou, 'Heat transfer by free convection between two parallel flat plates', *Numer. Heat Transfer*, **5,** 95–106 (1982).
6. E. M. Sparrow and L. F. A. Azevedo, 'Vertical-channel natural convection spanning between the fully-developed limit and the single-plate boundary-layer limit', *Int. J. Heat Mass Transfer*, **28,** 1847–1857 (1985).
7. E. M. Sparrow, G. M. Chrysler and L. F. Azevedo, 'Observed flow reversals and measured-predicted Nusselt numbers for natural convection in an one-side heated vertical channel, *J. Heat Transfer*, **106,** 325–332 (1984).
8. S. V. Patankar, *Numerical Heat Transfer and Fluid Flow*, McGraw-Hill, New York, 1980.
9. S. V. Patankar, 'A calculation procedure for two-dimensional elliptic situations', *Numer. Heat Transfer*, **4,** 409–425 (1981).
10. S. V. Patankar and D. B. Spalding, 'A calculation procedure for heat, mass and momentum transfer in three-dimensional parabolic flows', *Int. J. Heat Mass Transfer*, **15,** 1787–1806 (1972).
11. Y. Joshi and B. Gebhart, 'Transition of transient vertical natural convection flows in water', *J. Fluid Mech.*, **179,** 407–438 (1987).
12. B. Sammakia, B. Gebhart and Z. H. Qureshi, 'Measurements and calculations of transient natural convection in water', *J. Heat Transfer*, **104,** 644–848 (1982).
13. B. Sammakia, B. Gebhart and Z. H. Qureshi, 'Measurements and calculations of transient natural convection in air', *Int. J. Heat Mass Transfer*, **23,** 571–576 (1980).
14. D. A. Anderson, J. C. Tannehill and R. H. Pletcher, *Computational Fluid Mechanics and Heat Transfer*, Hemisphere, Washington DC, 1984, Chap. 4.
15. J. A. Schetz and R. Eichhorn, 'Unsteady natural convection in the vicinity of a doubly infinite vertical plate', *J. Heat Transfer*, **84C,** 334–338 (1962).
16. T. S. Chang and T. F. Lin, 'Transient buoyancy induced flow through a heated, vertical channel of finite height', *Numer. Heat Transfer* Part A, **16,** 15–35 (1989).
17. S. Ostrach, 'An analysis of laminar free-convection flow and heat transfer about a flat plate parallel to the direction of the generating body force', *NACA TN 2635*, 1952.